eLIFE elifesciences.org

RESEARCH ARTICLE

Figures and figure supplements

Defining the biological basis of radiomic phenotypes in lung cancer

Patrick Grossmann *et al*

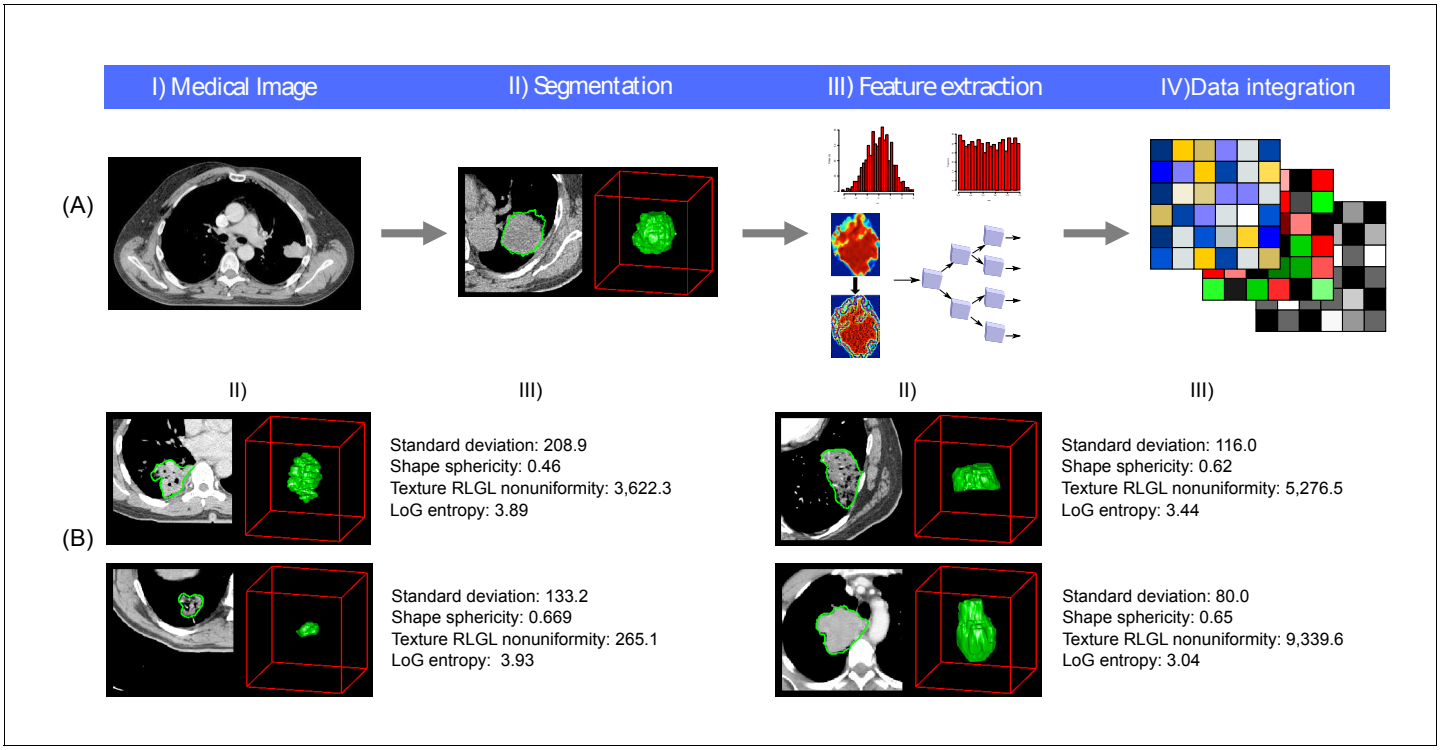

Figure 1. Radiomics approach. (**A**) Workflow of extracting radiomic features: (I) A lung tumor is scanned in multiple slices. (II) Next, the tumor is delineated in every slice and validated by an experienced physician. This allows creation of a 3D representation of the tumor outlining phenotypic differences of tumors. (III) Radiomic features are extracted from this 3D mask, and (IV) integrated with genomic and clinical data. (**B**) Representative examples of lung cancer tumors. Visual and nonvisual differences in tumor shape and texture between patients can be objectively defined by radiomics features, such as entropy of voxel intensity values ('How heterogeneous is the tumor?') or sphericity of the tumor ('How round is the tumor?').
DOI: 10.7554/eLife.23421.003

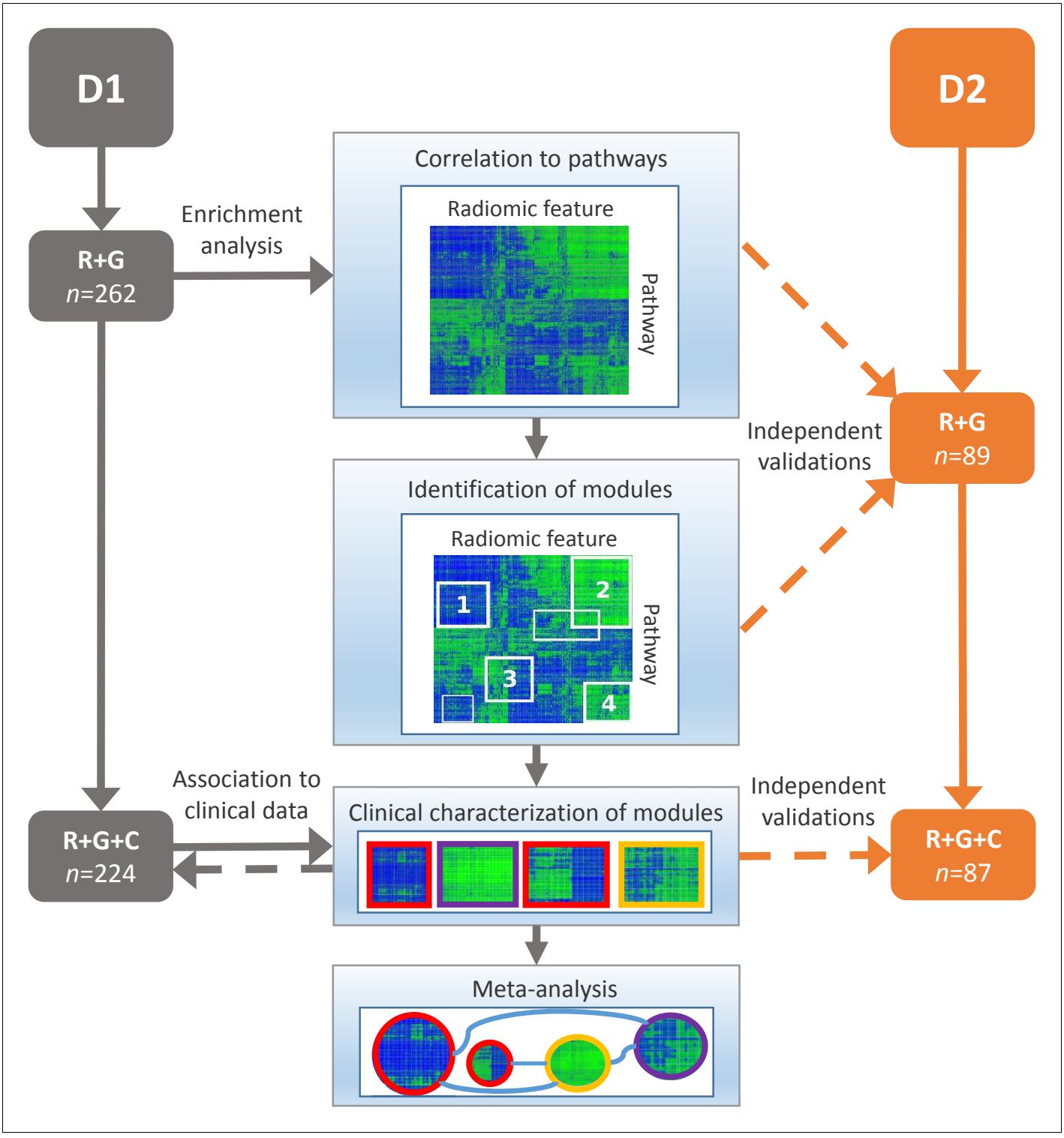

Figure 2. Schema of our strategy to define robust radiomic-pathway-clinical relationships. Two independent lung cancer cohorts (D1 and D2) with radiomic (R), genomic (G), and clinical (C) data were analyzed. D1 (n = 262) was used as a discovery cohort and D2 (n = 89) was used to validate our findings. A gene set enrichment analysis (GSEA) approach assessed scores for radiomic-pathway associations. These scores were biclustered to modules that contain features and pathways with coherent expression patterns. These modules may overlap and vary in size. Clinical association to overall survival (red), pathologic histology (purple), and TNM stage (yellow) was statistically tested in both datasets, and results were combined in a meta-analysis to investigate relationships of modules.

DOI: 10.7554/eLife.23421.004

Figure 2 continued on next page

Figure 2 continued

The following source data is available for figure 2:

Source data 1. Dataset1.
DOI: 10.7554/eLife.23421.005
Source data 2. Dataset2.
DOI: 10.7554/eLife.23421.006

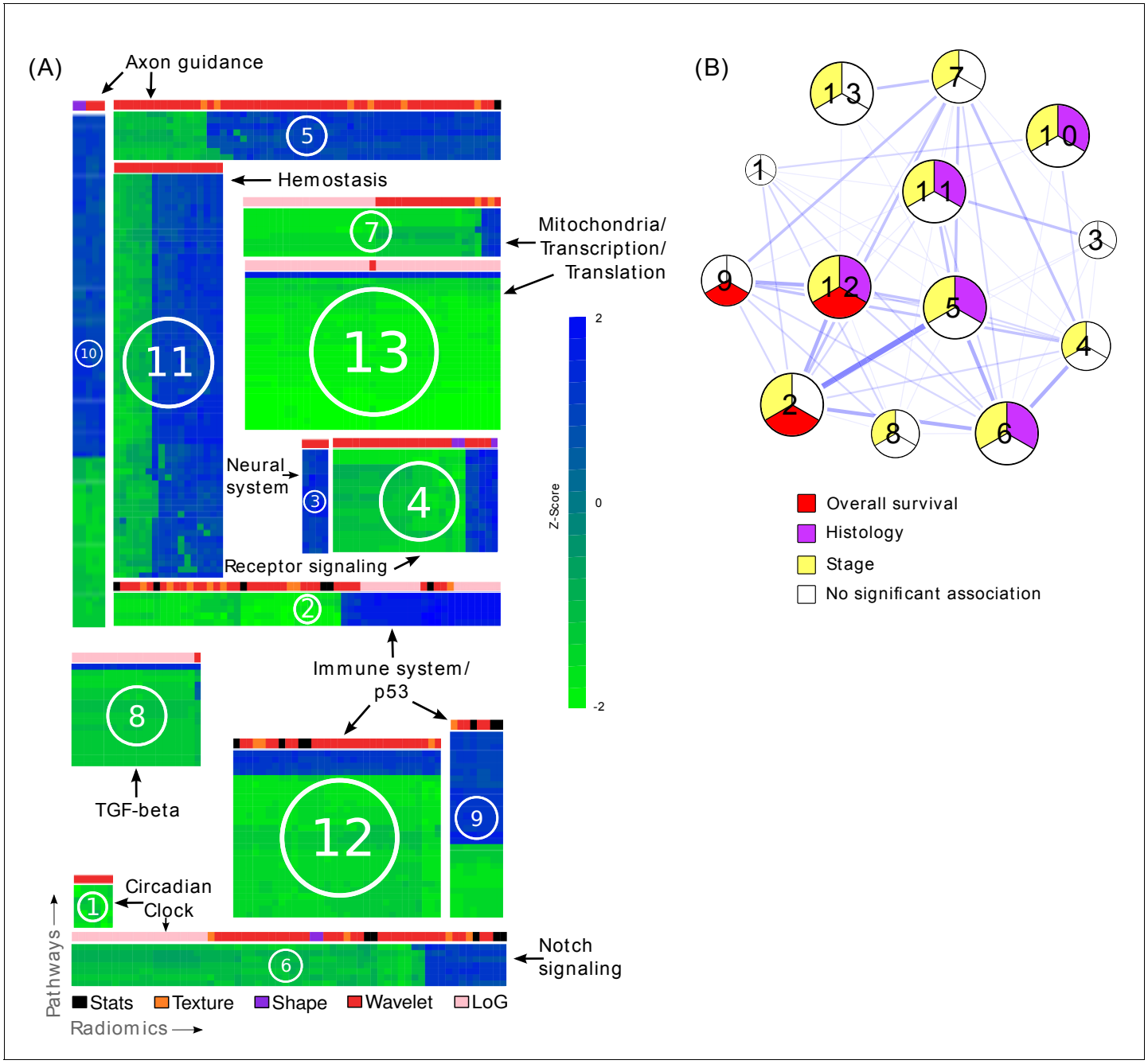

Figure 3. Radiomic-pathway-clinical modules. (**A**) Clustering of significantly validated radiomic-pathway association modules (FDR < 0.05). Normalized enrichment scores (NESs) have been biclustered to coherently expressed modules. Every heatmap in this figure corresponds to a module (M1 - M13) with radiomic features in columns and pathways in rows. Heatmap sizes are proportional to module sizes. Elements are NESs given in Z-scores across features, and are displayed in blue when positive and green when negative. Horizontal color bars above every module indicate radiomic feature groups (black = first order statistics, orange = texture, purple = shape, red = wavelet, and pink = Laplace of Gaussian). Representative molecular pathways are displayed. (**B**) Clinical module network. We investigated if modules were associated with overall survival (red), stage (yellow), histology (purple), or no clinical factor (white). Relationships of modules based on their number of shared radiomic features (thickness of blue lines) are displayed by a network. While we found that most modules yield clinical information, overlaps of modules did not indicate relationships to similar clinical factors.

DOI: 10.7554/eLife.23421.008

The following source data is available for figure 3:

Source data 1. Enlarged heatmaps of every module depicting normalized enrichment scores (NESs) of every pair of radiomic feature and molecular pathway clustered in a module.

DOI: 10.7554/eLife.23421.009

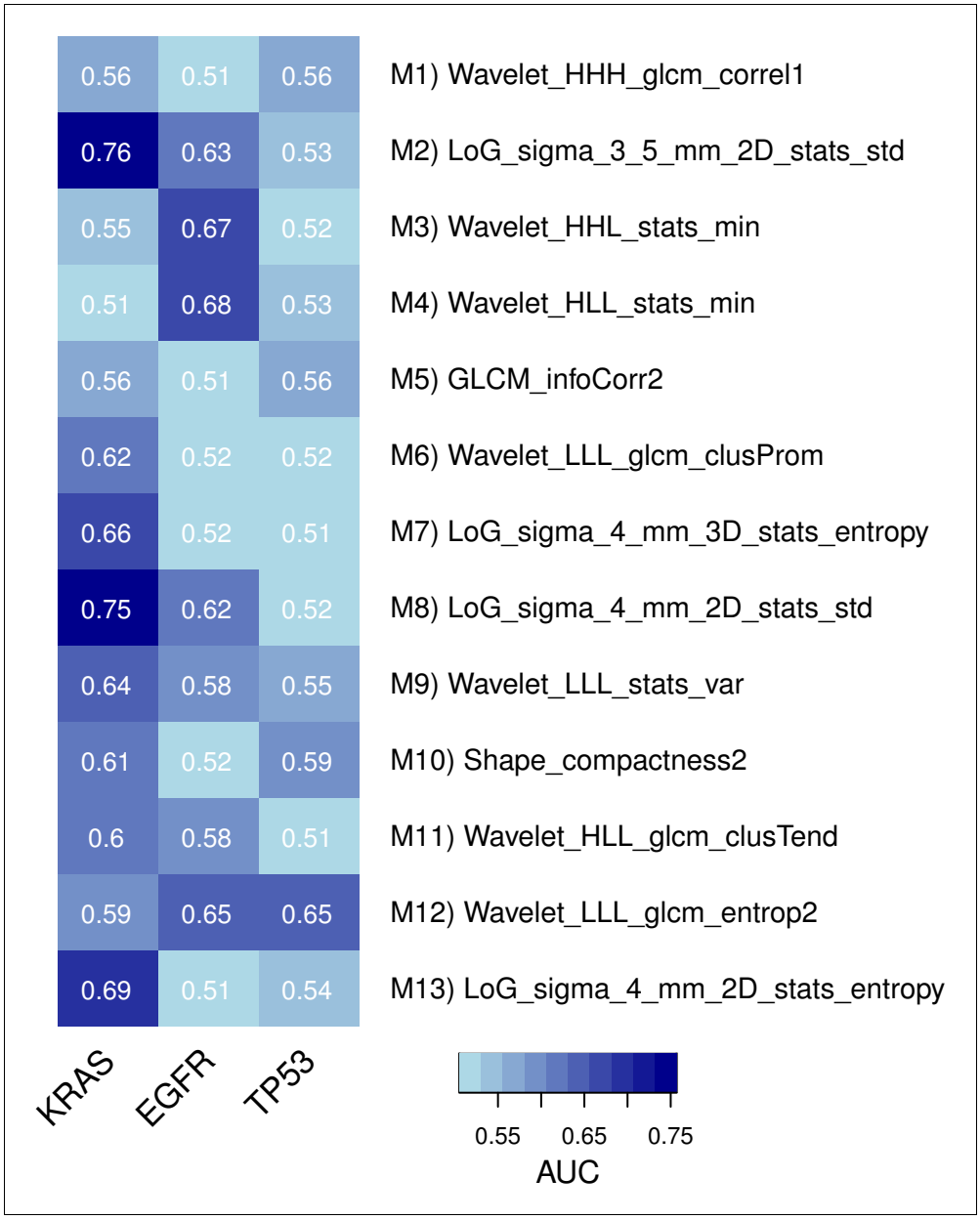

Figure 3—figure supplement 1. Predictive capabilities of representative radiomic features from every module for genetic mutations in KRAS, EGFR, and TP53 in a subset of the discovery cohort.
DOI: 10.7554/eLife.23421.010

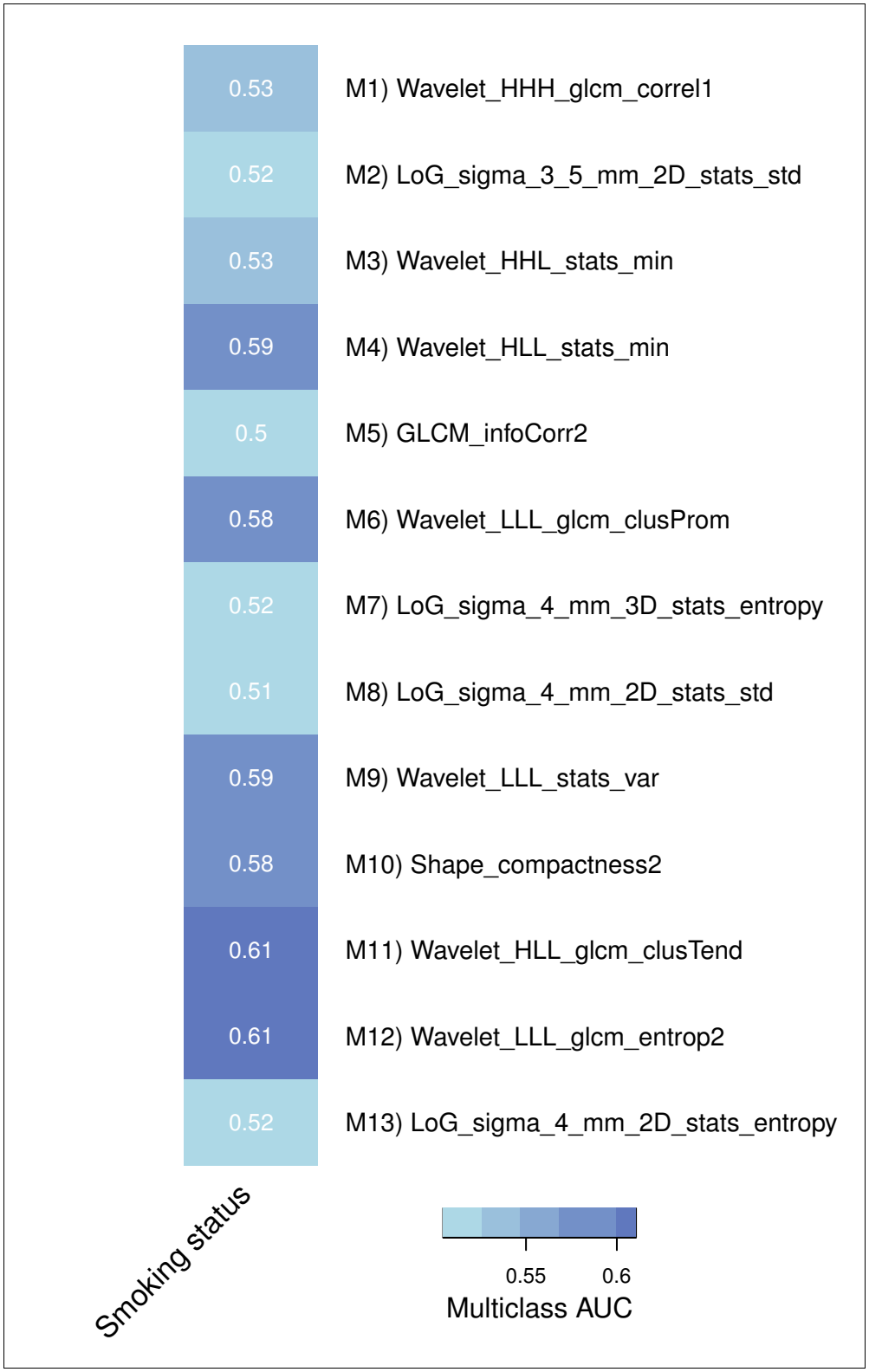

Figure 3—figure supplement 2. Association of representative features with smoking history in a subset of the discovery cohort.
DOI: 10.7554/eLife.23421.011

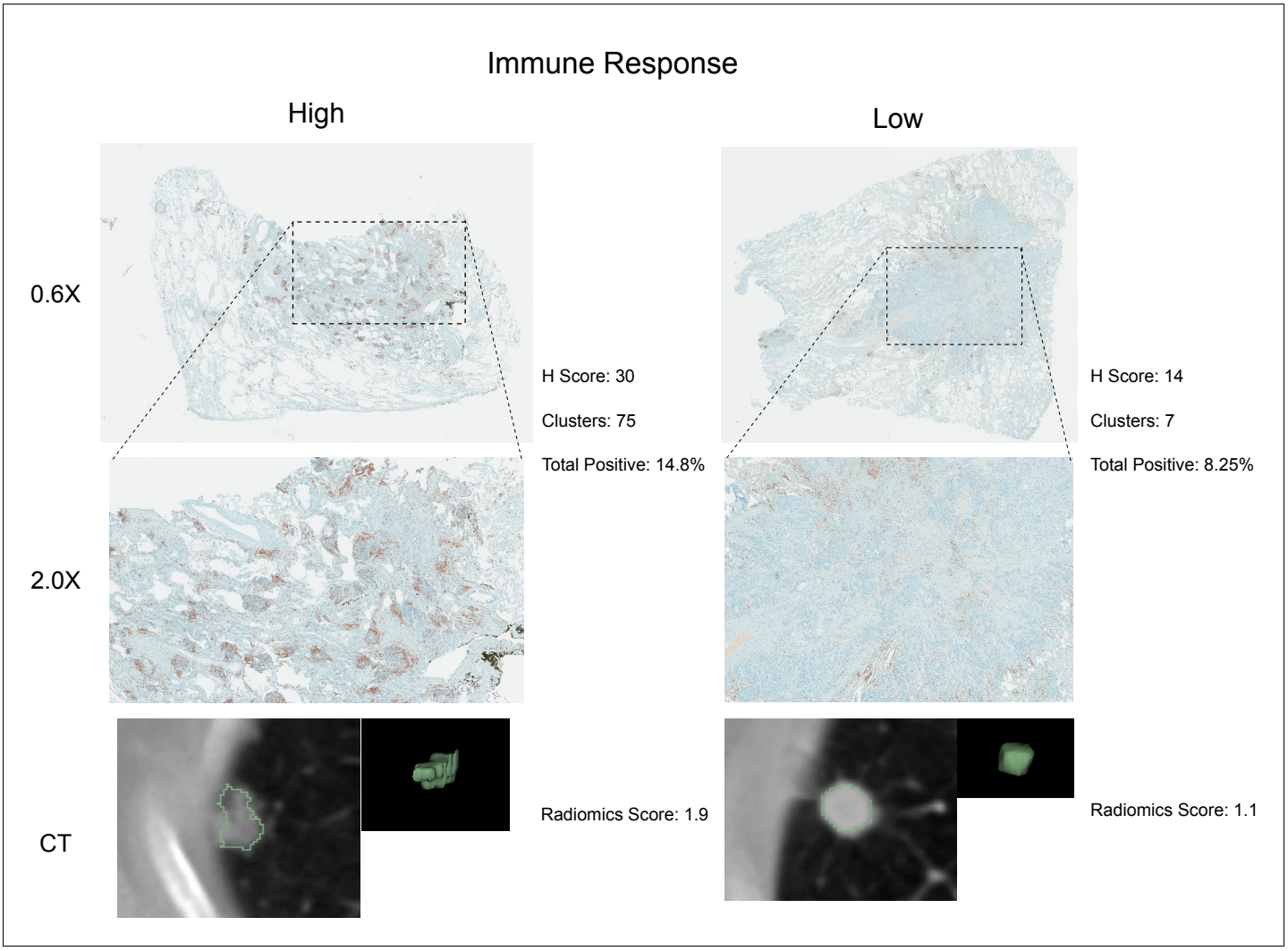

Figure 4. Test for agreement between radiomic and pathological immune response assessment. Two representative cases are shown where radiomic predictions of immune response were confirmed by immunohistochemical staining for nuclear CD3 highlighting lymphocytes in brown. Each case is displayed in 0.6X and 2.0X magnification of the tumor slides, and an axial slice of the corresponding diagnostic CT scan and the total tumor volume is given for comparison. Automated quantifications of lymphocytes are displayed in addition to the radiomics score incorporated to classify into high and low responders.

DOI: 10.7554/eLife.23421.015

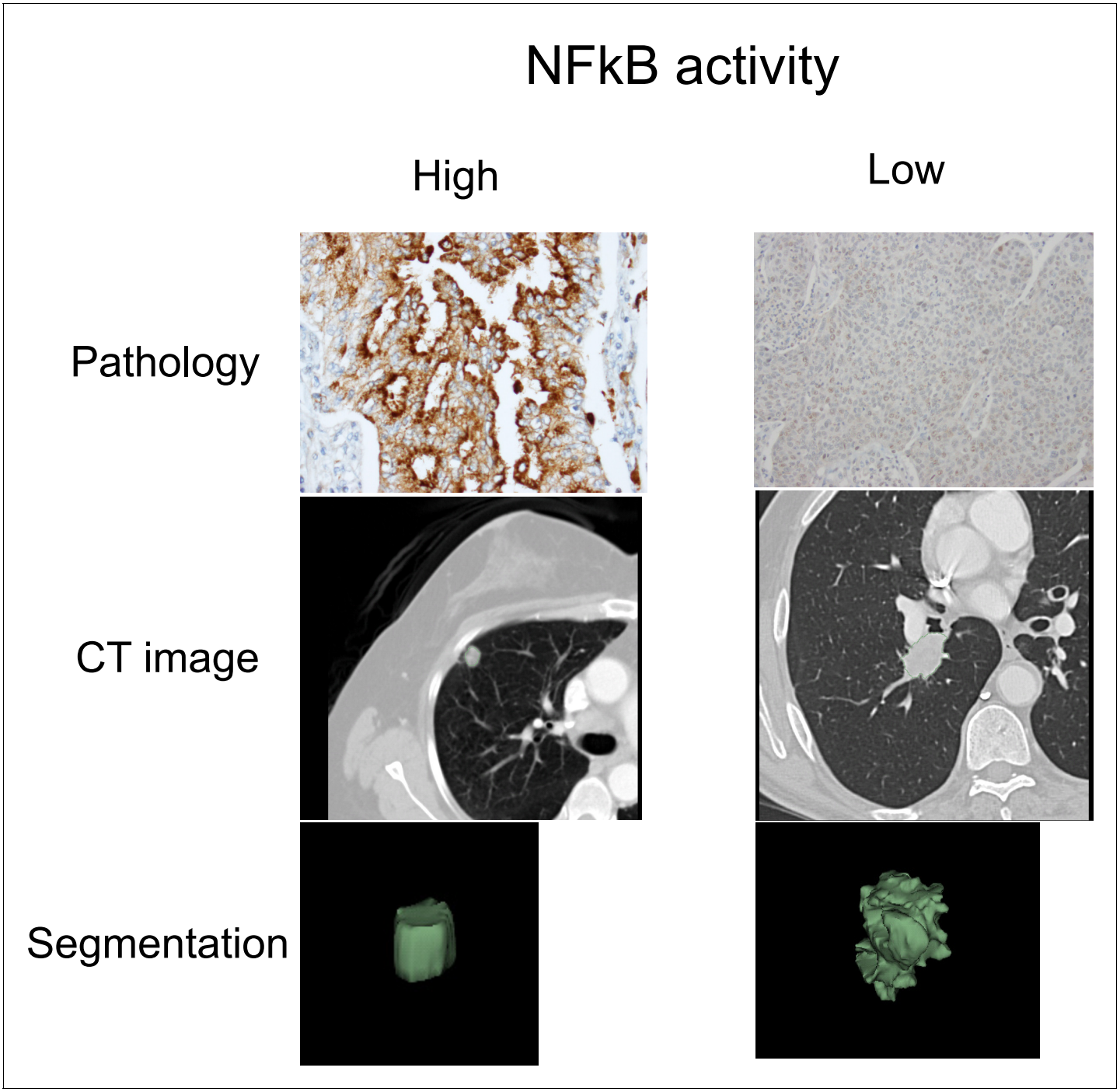

Figure 4—figure supplement 1. Representative cases of immunohistochemical staining for RelA.
DOI: 10.7554/eLife.23421.016

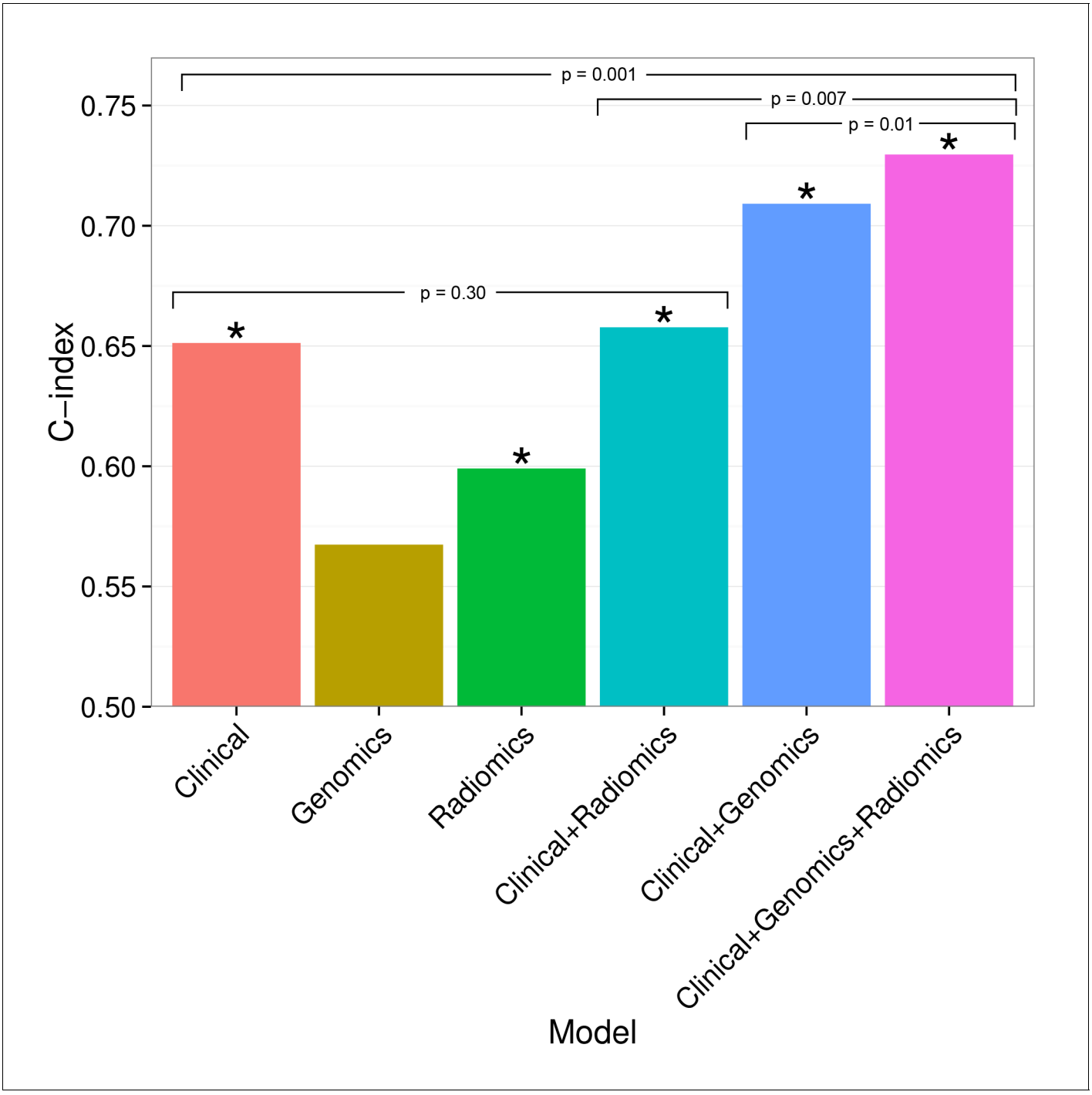

Figure 5. Combining prognostic signatures for overall survival. We tested combinations of clinical, genomic, and radiomic signatures. To a clinical Cox proportional-hazards regression model with stage and histology, we first added a published gene signature and next a published radiomic signature. These models were fitted on Dataset1 and evaluated with the C-index (CI) on Dataset2. An asterisk indicates significance ($p<0.05$). Combining different data types resulted in increased prognostic performances. By adding radiomic and genomic information, the initial performance of the clinical model was increased from CI = 0.65 (Noether p=0.001) to CI = 0.73 ($p=2\times10^{-9}$).

DOI: 10.7554/eLife.23421.017

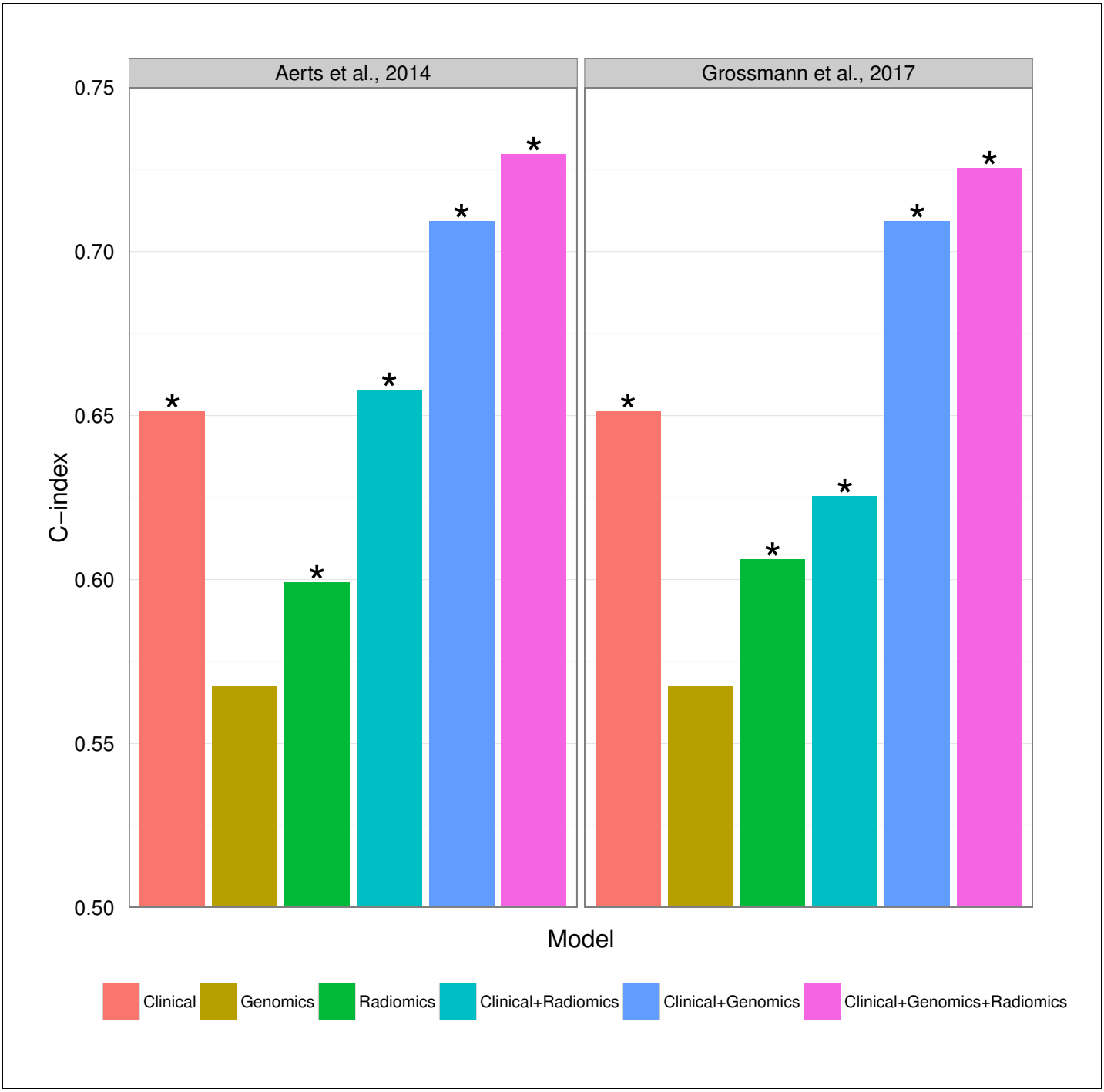

Figure 5—figure supplement 1. Prognostic performance of two radiomic signatures (i.e., a previously published and a novel signature) combined with genetic and clinical information.
DOI: 10.7554/eLife.23421.018

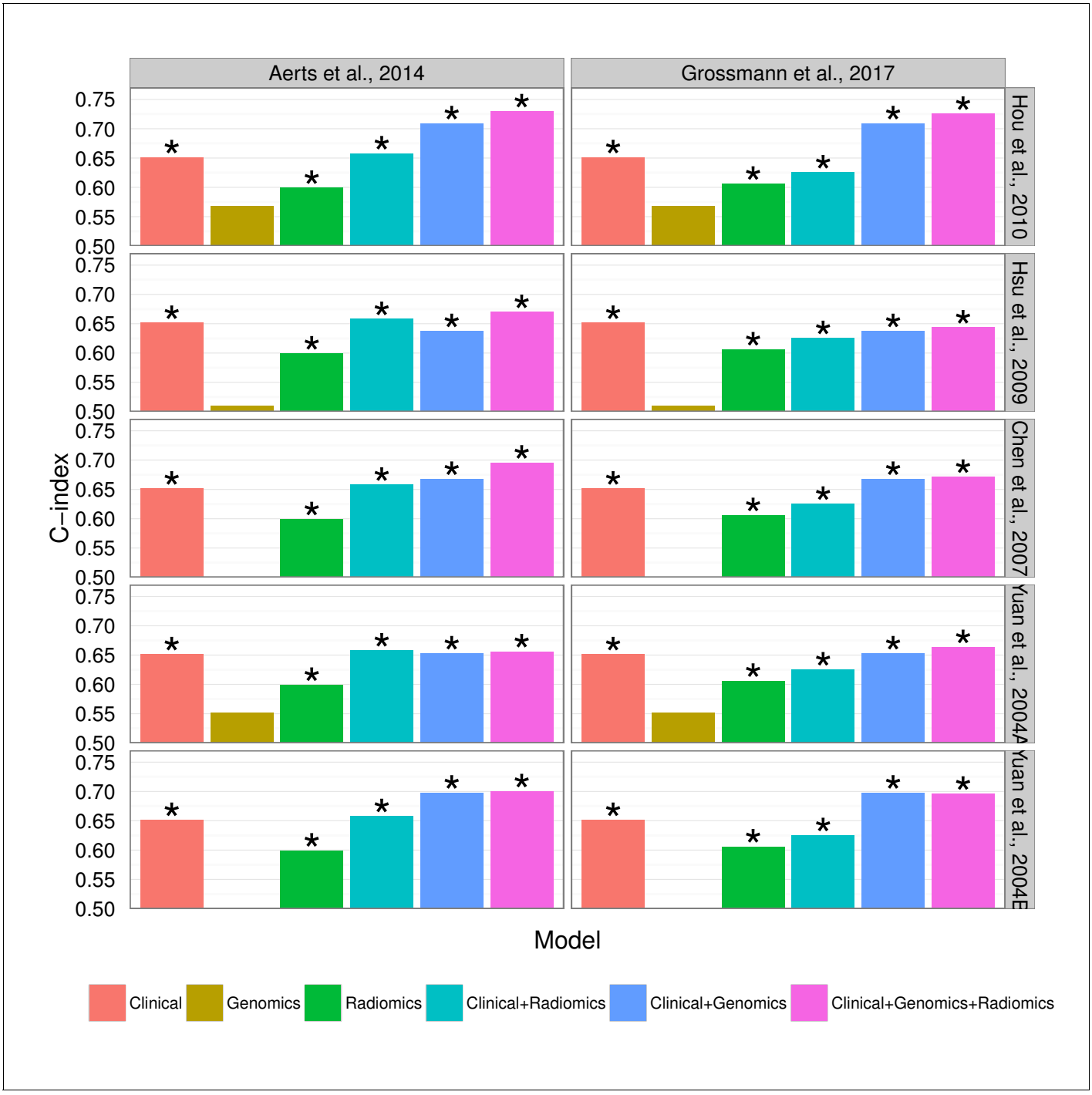

Figure 5—figure supplement 2. Prognostic performance of two radiomic signatures combined with different gene signatures and clinical information.
DOI: 10.7554/eLife.23421.019